(Received 24 May 2024, Accepted 7 November 2024, Scheduled 2 December 2024)

Millimeter-Wave Channel Measurements for 5G Networks Using a Low Cost Experimental Setup

Javier Enrique Arévalo Peña[1,*],
Juan Sebastián Chávez Martinez[1,2], and Javier Leonardo Araque Quijano[1]

[1]*Department of Electrical ans Electronics Engineering, Universidad Nacional de Colombia, Bogotá, Colombia*
[2]*Agencia Nacional del Espectro, Bogotá, Colombia*

ABSTRACT: This contribution presents the design and validation of a portable and low-cost experimental setup of a sounder for channel characterization at the millimeter wave band for 5G systems (Frequency Range 2-FR2). Unlike the high cost application-specific equipment employed by many research groups, universities, and telecommunication companies, which also requires adequate mounting and transport to and within the measurement sites, our channel sounder integrates several hardware and software components that result in a lightweight and convenient device for manual operation. Our device enables measurements at 26 GHz, a band earmarked for the upcoming deployment of 5G systems in the millimeter wave band in Colombia. We present channel measurements to validate the performance of the experimental setup and to assess the adherence to the predictions of the 3GPP (3rd Generation Partnership Project) TR (Technical Report) 38.901 standard propagation model, achieving favorable results.

1. INTRODUCTION

Wireless channel modeling is a valuable tool in the design and optimization of the performance and cost of radio networks. By leveraging accurate channel models, it is possible to predict key signal parameters, incorporating the effects of complex propagation phenomena. Hence, it is important to assess the accuracy of these models with reference to theoretical data, simulation data, and real-world measurements [1]. Specifically, millimeter wave communications exhibit unique propagation modeling challenges that warrant thorough investigation. These challenges include significant propagation loss due to atmospheric conditions, limited diffraction around obstacles, and reduced penetration capabilities, all of which are critical factors in the design and optimization of communication systems [2].

1.1. Experimental Channel Characterization

Research teams across various universities globally, as well as telecommunication service providers and equipment manufacturers, have conducted extensive measurements at millimeter wave frequencies. A concise overview of various experimental setups utilized for gathering data in diverse indoor and outdoor settings, as documented in the literature, provides a contextual foundation for the setup introduced in this study.

Based on Keysight commercial equipment, the authors of [3] suggested a millimeter wave MIMO channel sounding prototype system for 5G systems. Up to 40 GHz of frequencies are supported by the system, and larger frequency bands can be accommodated by adding more mmWave components.

Using a wideband sliding correlator channel sounder with steerable directional horn antennas at both the transmitter and receiver, the authors in [4, 5] provided experimental observations and empirically-based propagation channel models for the 28, 38, 60, and 73 GHz mmWave bands. A pyramidal horn antenna was attached to the RF waveguide output of the common design, which involved upconverting the baseband signal to an IF between 5 and 7 GHz and mixing it with a local oscillator to reach the proper mmWave band frequency for each campaign. After being mixed with a local oscillator to create an IF between 5 and 7 GHz, the received signal was then downconverted back to baseband using a rotatable pyramidal horn antenna that was attached to a waveguide flange input at the Rx.

A study of channel models and their authentications on the 26, 28, 36, and 38 GHz frequency bands for outdoor scenarios is presented in [6]. The continuous radio wave signal was produced at the TX side using a device called Anritsu MG369xC Series Synthesized Signal Generator. A vertically polarized, highly directional horn antenna was attached to the radio frequency's output. The vertically polarized horn antenna was connected to the Anritsu MS2720T high-performance handheld spectrum analyzer, which was running at zero spans, at the receiving (Rx) side in order to measure the received power level.

The measurements made with a high-performance vector signal generator that has a broad carrier frequency range are presented by the authors in [7]. The carrier frequency was set to 26 GHz for the measurements. A high-performance broadband vector signal analyzer is used at the Rx side. During the measurements, the transmitting (Tx) side employs three different antenna array topologies: a 64-element uniform linear array, a 64-element uniform planar array, and a 128-element uniform

* Corresponding author: Javier Enrique Arevalo Peña (jarevalop@unal.edu.co).

planar array. Vertical polarization biconical antennas with omnidirectional azimuthal patterns characterize both the transmitter and receiver. Prior to the measurements, GPS disciplines the calibrated rubidium clock at the Tx side, to which all clocks and sampling circuits in the transmitter and receiver systems were slaved.

In [8], the Tx is based on an Arbitrary Waveform Generator (AWG) to directly synthesize a modulated IF waveform. The IF signal is band-pass filtered, amplified, and up-converted using a phase-locked dielectric resonator oscillator, amplifier multiplier chain, and a mixer to a center frequency of 83.5 GHz. The system employs various transmitting antennas for calibration and field measurements. The channel sounder was designed for indoor and outdoor mobile radio measurements. To analyze the data, position, velocity, and heading of the antenna array are needed. For outdoor use, a GPS will be utilized. For indoor use, a robotic mobile positioning system is used to move the antenna array and provide this information.

The authors of [9–11] describe a narrowband sounder that used an omnidirectional antenna to receive a 28 GHz continuous wave (CW) tone in order to maximize the link budget and data gathering speed. The horn rotated in an azimuthal direction to gather signals coming in from all directions. The signal was then amplified by multiple Low Noise Amplifiers (LNAs) with adjustable gains, combined with a local oscillator. This produced an IF signal with an effective bandwidth of 20 kHz and a center frequency of 100 MHz. The power of the IF signal was measured, digitally converted using a power meter, and stored on a computer. The two horn antennas had a vertical polarization. A revolving platform held the entire receiver, including the data acquisition computer, enabling a complete angular scan at up to 300 r/min.

The complex Channel Transfer Function (CTF) in the frequency range of 25 GHz to 40 GHz was measured in [12] and [13] using a channel sounder implemented in the frequency domain by the Keysight N5227A Vector Network Analyzer (VNA). To automate the measurement process, a personal computer was used to control the positioning system and VNA.

Refs. [14, 15] use a commercial base station that is fixed inside the lab, an Ericsson AIR 5121 antenna, and 5G mobile router equipment (5G NR mmWave Mobile Hotspot) to enable measurements in the 28 GHz frequency band. The results show the coverage measurements and path loss results of a 5G indoor/outdoor channel.

1.2. mmWaves Channels for 5G Networks

Modeling of a channel at millimeter-wave frequencies can be performed deterministically in a site-specific environment validated through the comparison of detailed trajectory parameters with channel measurements and stochastically in broader generic environments validated by comparison of stochastic channel properties with channel measurements. In all of them, propagation phenomena such as diffraction, reflection, refraction, among others, are considered to be dependent on the operating frequency [16].

Among the deterministic models are the Ray Tracing Model, Map-Based Model, and t Point Cloud Model, which provide a characterization of multipath channels based on geometrical optics and uniform diffraction theory. The Ray Tracing Model uses GO (Geometric Optics) to calculate the direct, reflected, and refracted paths and uses GTD (Geometrical Theory of Diffraction) and UDT (Uniform Theory of Diffraction) to calculate the diffraction paths. For each path, the complex amplitude, delay and departure, and arrival angles of the signals are obtained. The accuracy of the ray tracing depends largely on the detailed description of the propagation environment including the physical structure of the objects and their electromagnetic parameters, and on the accuracy of the high frequency approximation implied in this formulation (small wavelength compared to all objects and relevant characteristics of the scenario) [17].

The Map-Based Model, a model proposed within the METIS (Mobile and wireless communications Enablers for the Twenty-twenty Information Society) project, is based on ray theory employing a simplified three-dimensional geometrical description of the propagation environment to account for propagation phenomena such as specular reflection, diffraction, scattering, and blocking. This model provides accurate and realistic channel properties, and is suitable for evaluating massive MIMO and beamforming systems [18].

The Point Cloud Model uses ray theory to characterize the propagation environment with higher accuracy. A laser scanning method can be used to obtain point cloud data of the propagation environment with more detailed object structure information. These data are then filtered to obtain a representation of the surface and proceed to calculate parameters such as amplitude, delay, and angle of the signals from the propagation phenomena such as specular and diffuse reflections [19].

Among the stochastic models, widely used for channel modeling in millimeter-wave bands, are the Saleh-Valenzuela (SV)-Based Model, Propagation Graph Model, and Geometric Based Stochastic Model in millimeter-wave bands (GBSM). The SV-Based Model is used to model the Channel Impulse Response (CIR). It assumes that the rays arrive in clusters with delays following a Poisson distribution (exponential distribution for the inter-arrival times). Then, the CIR can be described by parameters such as cluster power decay rate, lightning power decay rate, cluster arrival rate, and lightning arrival rate. With modifications the SV-Based Model has been extended and adopted by IEEE 802.15.3c and IEEE 802.11ad [20].

The Propagation Graph Model is based on graph theory in which in a propagation graph the transmitters, receivers, and scattering elements are represented by vertices, and the propagation conditions between the vertices are represented by edges with probability values. The angle information is also obtained from the distribution of the network elements [21].

The GBSM is classified into RS (Regular Shaped) GBSM and IS (Irregular Shaped) GBSM. In RS GBSM, regularly shaped scatterers with one ring, two rings, ellipses, cylinders, and others are assumed, and in IS GBSM, irregularly shaped scatterers are used. In general, this model, widely applied to different scenarios, has been used in channel model proposals presented by several international organizations and research groups for millimeter-wave frequencies, among which the following can be named:

1. Mobile and wireless communications Enablers for the Twenty-twenty Information Society (METIS): It is an extensive research project funded by the European Union that was based on the earlier WINNER II and WINNER+ channel models. The METIS project proposed a stochastic model for frequencies up to 70 GHZ and a Map-Based model, presented above, applicable up to 100 GHz, as well as hybrid models. It is applicable to a wide range of indoor and outdoor scenarios, such as Urban Macrocell (UMa), Urban Microcell (UMi), Device to Device (D2D), Vehicle to Vehicle (V2V), rural, road, indoor, shopping malls, and offices [22].
2. Millimeter-Wave Based Mobile Radio Access Network for 5G Integrated Communications (mmMAGIC): It is another extensive research project funded by the European Union under the 5G Partnership initiative bringing together major contributions from industrial companies. It takes into account the main changes in mobile systems to support dense networks with a high degree of flexibility and performance, covering frequencies from 6 GHz to 100 GHz [23].
3. New York University (NYU) WIRELESS Model: It is a project of the New York University at NYU Tandon School of Engineering based on the 3rd Generation Partnership Project (3GPP) TR 38.901 model that uses a database of downtown New York City characterized by more realistic results for urban scenarios [24].
4. QUAsi Deterministic Radio channel GenerAtor (QuaDRiGa) Model: It is a model proposed by Fraunhofer Institute for Telecommunications as a 3D extension of the WINNER model. It is an open access platform that although initially used for simulations of frequencies below 6 GHz, it can be used for simulations in millimeter-wave frequency bands [25].
5. Millimeter-Wave Evolution for Backhaul and Access (miWEBA): It is a 3D channel model that was proposed for the 60 GHz band applicable to D2D scenarios and specific types of mobile access such as university campuses, streets, hotel receptions. It is a hybrid model that combines measurement parameters with existing channels in order to characterize the multipath components of the weak and strong multipath components of the channel [26].
6. 3GPP Reference Model Channel: Finally, 3GPP TR 38.901 presents several propagation models, applicable in the 500 MHz–100 GHz band, intended to calculate different variables of interest for the simulation and design of wireless communications networks, such as path loss, line-of-sight probability, shadow fading, building penetration loss, and some other aspects of interest, clearly detailing how to obtain the input parameters of each model [27, 28]. The technical information is framed within four main scenarios of interest, which are listed below:

(a) RMa: This is a rural deployment scenario that focuses on extensive and continuous coverage. The key features of this scenario are wide-area continuous coverage that supports high-speed vehicles. This scenario is limited by noise and/or interference.

(b) UMi with Outdoor-to-Outdoor and Outdoor-to-Indoor propagation: A scenario in which base stations are mounted below the rooftop levels of surrounding buildings. UMi's open area is intended to capture real-life scenarios, such as a city or a station plaza. The width of the typical open area is on the order of 50 m to 100 m.

(c) UMa with Outdoor-to-Outdoor and Outdoor-to-Indoor propagation: acbs are mounted on the rooftop levels of the surrounding buildings and can also represent a rural area, where the buildings are low, and the base stations are high to cover a large area.

(d) Indoor: This scenario is designed to capture various typical indoor deployment scenarios, including office environments and shopping malls. The typical office environment consists of open cubicle areas, offices with walls, open areas, corridors, etc. Base stations are mounted 2–3 m high on ceilings or walls. Business centers are typically 1–5 stories high and may include an open area shared by several floors. Base stations are mounted at a height of approximately 3 m on the walls or ceilings of corridors and stores.

This study makes several key contributions to the field of mmWave band channel characterization, including: i) the detailed description of the design and experimental validation of an open, flexible, and cost-effective platform for channel characterization in the mmWave band; ii) the development of a platform that facilitates manual transport and operation, closely mimicking the experience of a mobile communication user in realistic scenarios; iii) to the best of our knowledge, this work represents the first instance of radio channel measurements in the millimeter wave band conducted in Colombia, significantly preceding the anticipated rollout of 5G systems in the FR2 band within the country; iv) the evaluation of experimental results through comparison with a standard propagation model, offering valuable insights into the application of such models in the design of 5G FR2 wireless networks, particularly in the context of Colombia's unique atmospheric, urban, and topographic conditions.

2. CHANNEL SOUNDER ARCHITECTURE AND DESIGN

In this section, we describe the design of our experimental testbed using a bottom up approach. The testbed is composed by, going from the air interface backwards: millimeter wave transceivers, baseband processor, various position tracking devices, and a processing unit. Such a setup is replicated at both sides of the channel, whereby a base station device is static and provides a stable radio signal and an accurate positioning reference, and a rover device is used to move through the area of study. In the following, these blocks are described in detail.

2.1. Transceivers

For the generation and reception of waves in the desired band, two transceivers from the manufacturer Sivers Semiconductors are used, developed for experimentation and channel study in a band from 24 GHz to 29.5 GHz [29]. These devices feature two 2×8 patch antenna arrays, one for transmission and an identical array for reception, which provide a narrow beam in the horizontal plane and a wide beam in the vertical plane. These devices also include an analog filter in their reception mode that suppresses out-of-band interference, making it a robust device in a noisy environment. This device includes a software package developed in Python that allows the modification of some parameters of interest, such as central frequency, vertical and horizontal beam orientations, gain, among others, either through console commands or a graphical interface. This device does not transmit/receive signals generated by itself; instead, it takes/produces baseband signals in differential mode through its I-Q I/O ports, which are the baseband version of the transmitted/received signal in the radio band of interest. The EVK02001 transceiver shown in Fig. 1 used in the measuring process has the following features:

- Beamforming capability with 16 transmitting channels and 16 receiving channels. Beam steering with patch antenna array, azimuth: ±45°.
- Integrated synthesizer compatible with 5G NR OFDM modulation up to 64 QAM and SC modulation up to 256 QAM depending on baseband capabilities.
- Output transmitting power of approx. 45 dB and antenna array gain of approx. 20 dBi.
- Support for RF channels up to 2 GHz and additional support for split RF channels (1/2 and 1/4 channel).
- Optimized for 3GPP NR 5G fixed wireless access applications Compatible with IEEE 802.11ad standard, MCS0-12 modulation.

FIGURE 1. Transceiver EVK02001 (parch antenna 2×8).

2.2. Baseband Processor

For the generation and reception of the aforementioned baseband signals, Ettus B210 reference USRP devices are used. These devices provide a fully integrated Software-Defined Radio (SDR) platform, with continuous frequency coverage from 70 MHz to 6 GHz in real-time. The manipulation of this device is possible thanks to the USRP Hardware Driver™ (UHD), available for programming languages such as C++ or Python, as well as more specialized software like GNU Radio, MATLAB, or LabVIEW. This device possesses a 2×2 transceiver arrangement very well suited to connect to the differential IQ ports of the mmWave transceiver.

2.3. GPS Modules

Because path losses are described as a function of the distance between the transmitter (Tx) and receiver (Rx), it is necessary to include in the experimental setup a device capable of obtaining this parameter. For this purpose, two C94-M8P-2 modules from the manufacturer U-Blox were used [30]. Although these devices can function independently, their optimal performance is achieved when they operate in pairs. One is configured as the "base station" with a fixed coordinate and the other as a "rover", acting as a mobile device that utilizes its own location, obtained through GNSS readings, and correction messages received from the "base station" to provide a position in terms of coordinates or relative position accuracy compared to the fixed "base station", improving the precision achieved by GNSS readings alone by a factor of ten or better. In our tests we verified centimeter positioning accuracy.

2.4. Magnetometer Accelerometer

Although only the variables measured by the aforementioned instruments are necessary for an accurate estimation of path losses, an additional element was chosen to be added to the test setup: a magnetometer and accelerometer positioned on the reception transceiver. This placement allows for determining the full 3-D orientation of the rover antenna, thus aiding in the correct alignment of both antenna arrays during the measurement and in the computational removal of errors due to antenna misalignment from knowledge of the antenna pattern. The GY-511 module was used for this purpose, equipped with I^2C communication pins and compatibility with various platforms such as Arduino or Raspberry Pi. Additionally, it comes with supporting software for each of these different platforms.

2.5. Processing Unit

For the purpose of achieving a compact and portable setup while collecting data from the previously mentioned equipment, the Raspberry Pi 3 Model B board was selected. This device is a versatile mini-computer that supports a broad range of GNU/Linux-based operating systems. It is equipped with multiple connectivity options, including four USB 2.0 ports, an Ethernet port, an HDMI port, and others, which facilitate the interaction with various devices. Moreover, it features a set of GPIO pins that enable its use as a programmable controller for diverse robotics or electronics projects. Among these pins

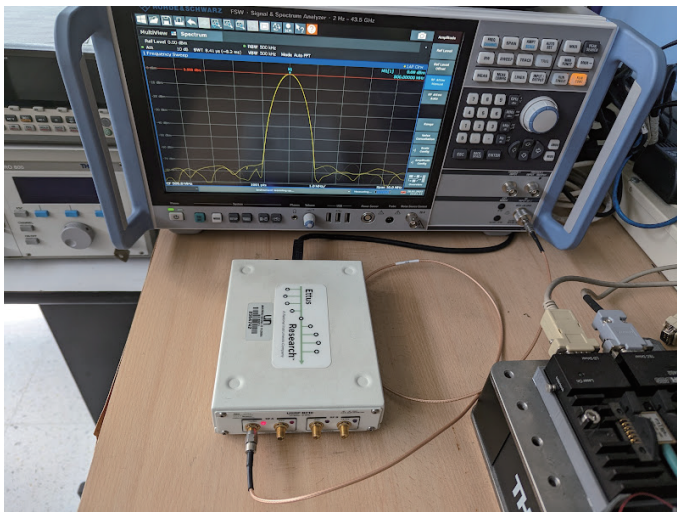

FIGURE 2. Calibration setup for the baseband module in the transmitter (BS) node.

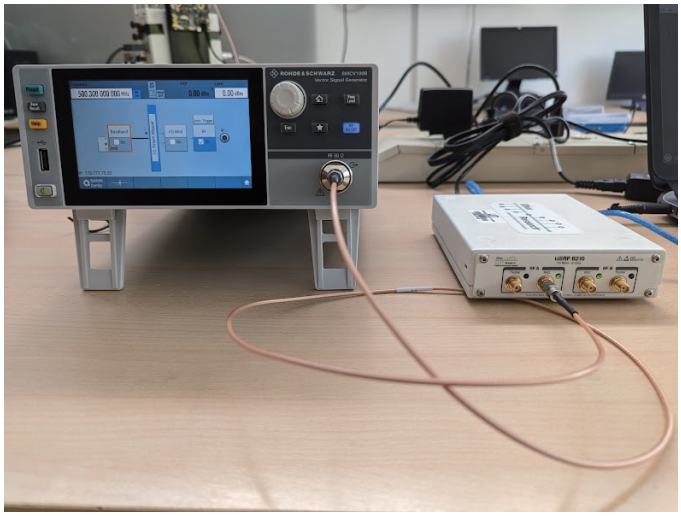

FIGURE 3. Calibration setup for the baseband module in the receiver (rover) node.

are the I^2C and SPI communication ports, which are instrumental in managing external devices. The choice of this device is driven by its ability to efficiently control all the mentioned equipment, coupled with its compact size that contributes to the development of a lightweight rover unit. Furthermore, its low power consumption allows for extended operations powered by a modestly sized battery bank, eliminating the need for frequent recharging.

3. EQUIPMENT CALIBRATION

The calibration process is essential for both baseband and mmWave transceivers, as they do not provide readings or output signals in absolute voltage or power values. Instead, the values accessed through the software interface (e.g., GNU Radio/MATLAB) are referenced to an internally defined unit that is initially unspecified. To address this, a characterization procedure is undertaken to accurately determine the scaling factors. These factors are crucial for our measurement campaign, ensuring the precision and reliability of the data collected.

According to the manufacturer's recommendation for the baseband processor [31], a simple method for calibration involves using another previously calibrated device. For the transmitting module, the output of the USRP B210 is connected to a spectrum analyzer, as illustrated in Fig. 2 adjusting the gain of the output signal until a power of 0 dBm is achieved. Similarly, the baseband processor used for reception is calibrated with the assistance of a vector signal generator, as shown in Fig. 3. With this setup, the reference level of the USRP is calculated based on the amplitude of the recorded signal and the known power of the input signal.

For the calibration of the transceivers, the setup shown in Fig. 4 is used, where the output of the Rx transceiver is connected to a spectrum analyzer. All preconfigured gains in both Tx and Rx transceivers are varied to identify the individual contribution of each, subsequently taking them into account in the calculation of path losses.

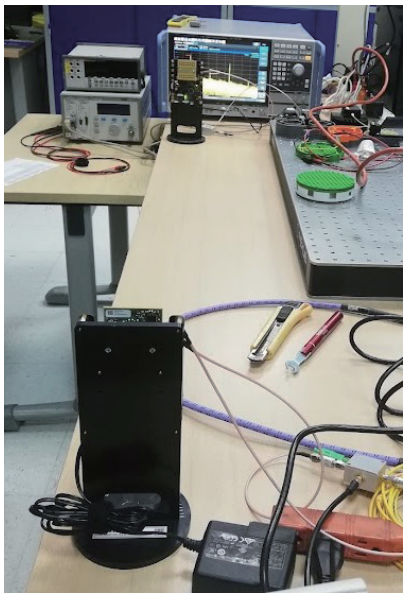

FIGURE 4. Calibration setup for the millimeter wave transceivers.

4. MEASUREMENT MODULES

4.1. Tx Module

The transmission module, whose diagram is shown in Fig. 5, consists of 4 devices: a computer, a USRP, a C94-M8P-2 module, and a transceiver. The computer is responsible for initiating processes on the other devices; from it, the GPS receiver is configured in "base station mode", assigning it a fixed coordinate. Additionally, the transceiver's Tx mode is initialized, specifying its central frequency, beam orientation, and gain. The USRP is also configured in transmission mode to generate a baseband signal to feed the transceiver.

With this module initialized, the GNSS device starts generating and wirelessly transmitting positioning reference data, which will be utilized by the "rover" to obtain an accurate loca-

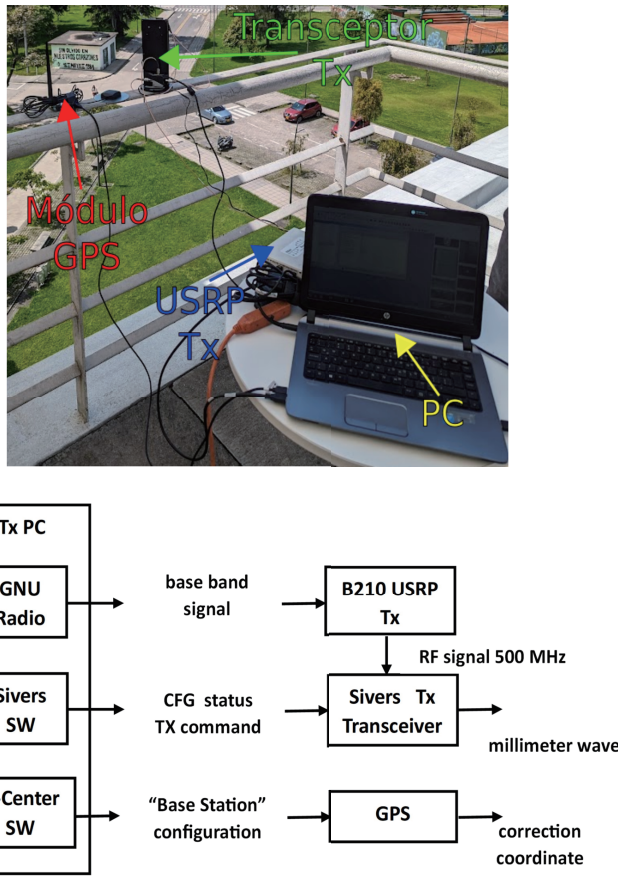

FIGURE 5. Photograph and block diagram of the transmission (base station) Node.

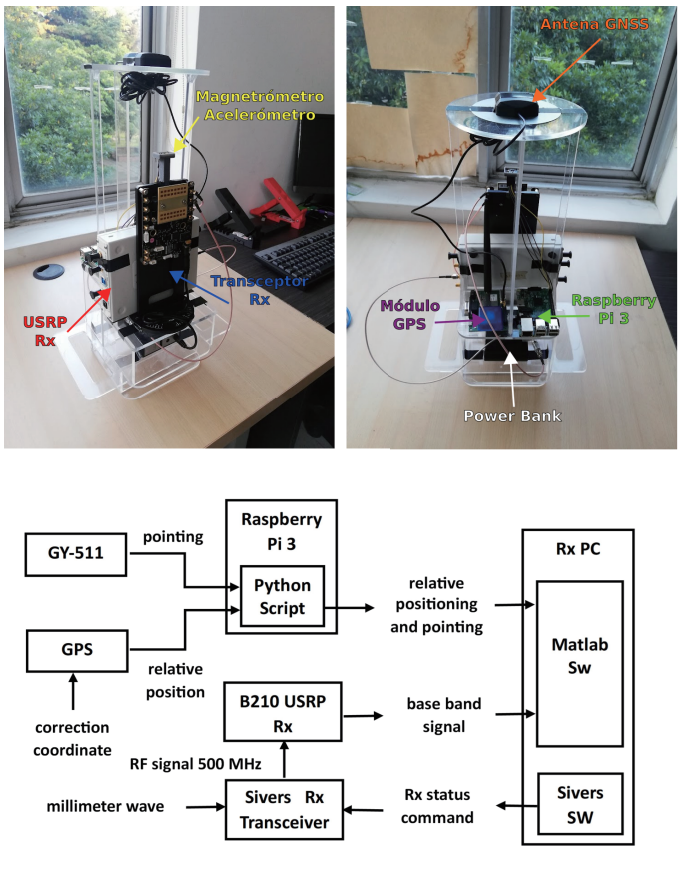

FIGURE 6. Photograph and block diagram of the reception (rover) node.

tion. Through GNU Radio, the USRP is configured to output a sinusoidal signal with a power of 0 dBm and a central frequency of 500 MHz on its output ports. This signal will be taken to the differential I-Q terminals of the transceiver, where it will be modulated and transmitted at a frequency in the millimeter-wave band.

4.2. Rx Module

In the Rx module, as shown in Fig. 6, the C94-M8P-2 module, configured in rover mode, receives messages sent from the base station to provide more precise positioning. Meanwhile, the GY-511 magnetometer and accelerometer read the horizontal and vertical alignment. These two instruments are read through a Python script executed from the Raspberry Pi, and the data is then sent to the PC via a MATLAB routine. Conversely to the base station device, the transceiver in the rover receives the signal in the millimeter-wave band, demodulates it, and delivers it to the USRP in baseband frequency. This, in turn, is read using the same MATLAB routine used to measure the other variables so that data from all three measured variables are collected during the measurement period.

5. DESCRIPTION OF THE MEASUREMENT CAMPAIGN

The conducted experiment involved generating a signal with known characteristics using the Tx module and subsequently receiving this signal using the Rx module. The aim was to compare the two signals to determine the path losses of the wave in the medium, based on the frequency of the wave and the distance between the transmitting and receiving antennas. To achieve this, the Tx module was positioned at a height of 11 m above ground level, while an operator held the Rx module at a height of 1.5 m. The operator then walked in a straight line away from the position of the Tx module, always ensuring proper alignment between the antennas of both modules and moving to the farthest distance possible while maintaining line of sight between Tx and Rx. Fig. 7 depicts the path taken by the operator, which represents the geographic layout of our experimental setup, highlighting the spatial relationship between the base station and the various measurement points across the study area in yellow and blue colors, respectively.

This experiment was conducted between 10 am and 1 pm on a day with an approximate temperature of $17°C$ and 60% humidity.

Data acquisition is performed through a MATLAB routine that implements a reading loop. During each cycle, data from

FIGURE 7. Map illustrating the distribution of measurement locations marked by blue points and the location of the base station indicated by a yellow point.

the three variables of interest are received. This includes measuring alignment (measured as two angles, one for vertical alignment and one for horizontal alignment), the rover's relative position to the base station (measured as relative position in latitude, longitude, and altitude), and the measurement of a data frame from the USRP. These frames consist of 4096 samples, taken at a sampling frequency of 2 MHz. This method allows for multiple measurements from the instruments per second. Once the measurement is completed and the data saved, a calculation is performed to obtain the power of the received signal for each distance point, applying the results obtained from the previously explained calibration. This allows obtaining a measurement of path losses as a function of the distance between the transmitter and receiver.

6. RESULTS AND DISCUSSION

Our report of this study's findings centers around the measurements taken and their comparison with the 3GPP TR 38.901 reference model at the key frequency of 26 GHz, depicted in Fig. 8. Furthermore, to provide a comprehensive evaluation of the experimental setup's performance, results at adjacent frequencies are also explored: the lower frequency of 24.5 GHz, illustrated in Fig. 9, and the higher frequency of 26.5 GHz, shown in Fig. 10. This analysis across a spectrum of frequencies offers a detailed insight into the setup's effectiveness. The initial findings affirm the experimental setup's functionality, as evidenced by the observed increase in losses correlating with the distance between the antennas. This trend aligns with the expected behavior outlined by the 3GPP model's path loss equation, indicating a consistent increase in losses with distance. However, despite these similarities, notable discrepancies emerge between the actual measurements and the theoretical propagation model, particularly at distances up to approximately 50 meters. These differences highlight areas for further investigation to understand the causes of deviation from the model predictions. A notable observation is the discrepancy in behavior

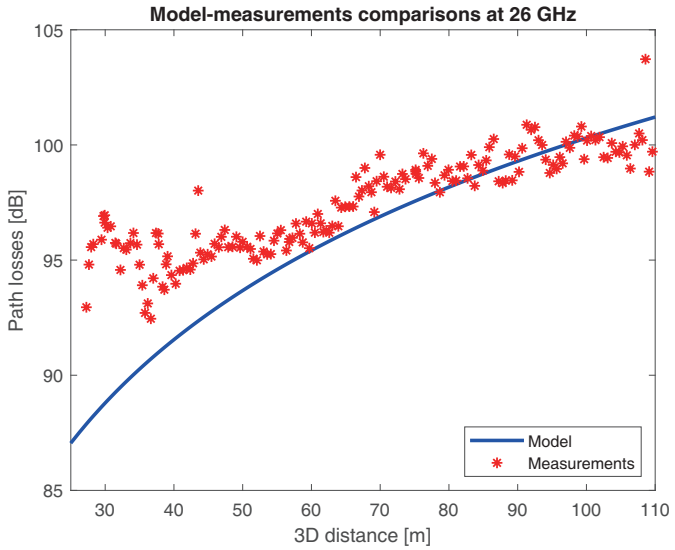

FIGURE 8. Path loss measurements at 26 GHz and comparison with the 3GPP TR 38.901 model.

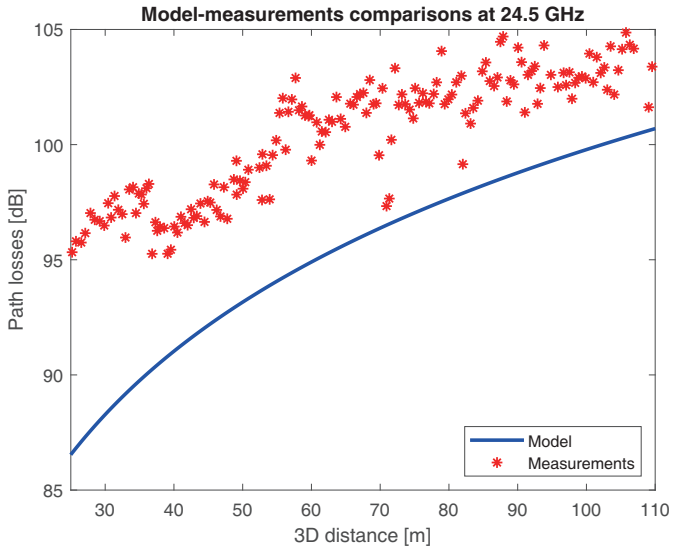

FIGURE 9. Path loss measurements at 24.5 GHz and comparison with the 3GPP TR 38.901 model.

at 24.5 GHz, where the measured path loss deviates markedly from that predicted by the theoretical model, indicating a much greater loss than anticipated. Despite thorough and repeated verification of the experiment, no errors were found. This suggests the possibility of atmospheric absorption or another environmental factor at this specific frequency contributing to an elevated level of path loss. Such an anomaly merits additional exploration in subsequent studies to better understand the underlying causes. At the primary frequency of 26 GHz and the higher frequency of 26.5 GHz, the observed losses closely align with those projected by the theoretical model, albeit with an additional loss ranging between 1 dB and 4 dB beyond the anticipated values. This discrepancy could stem from a variety of reasons, including unique channel characteristics specific to the measurement environment or potential inaccuracies in the mea-

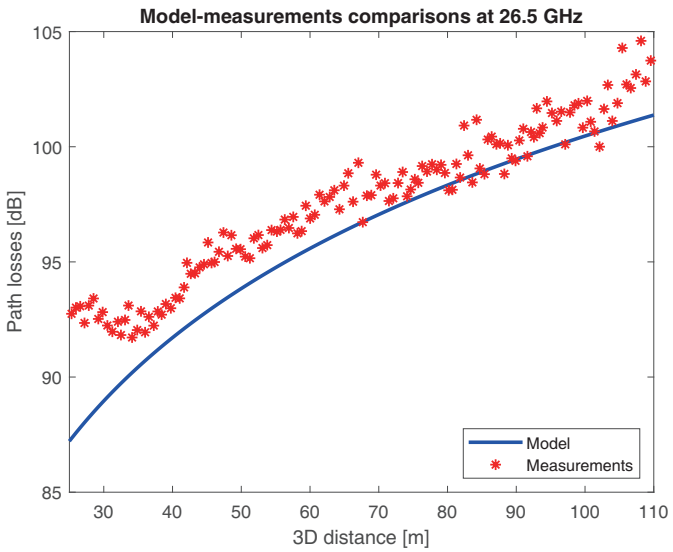

FIGURE 10. Path loss measurements at 26.5 GHz and comparison with the 3GPP TR 38.901 model.

surement process itself. Nonetheless, this variance is deemed minor and can be readily adjusted in the 3GPP model's equation by incorporating an offset, thereby aligning the model more closely with the observed results. An additional observation is that measurements display a slower loss rate at large distances that could considerably impact the coverage predictions based on the model alone.

7. CONCLUSIONS

The deviations observed between empirical measurements and the theoretical model carry significant implications for wireless network designers, particularly in the realms of network capacity planning and optimization. These discrepancies not only reveal the potential for miscalculating network needs — leading to either under-provisioning, which could degrade service quality, or over-provisioning, which could inflate costs unnecessarily — but also highlight the critical role of extensive measurement campaigns in mitigating such risks. The insights gained from this study reflect on the broader necessity of aligning practical deployments with theoretical expectations, thereby ensuring that network design and deployment strategies are both cost-effective and performance-optimized.

Considering our findings, our future work will leverage the versatility of our experimental setup, to extend our measurement campaigns to cover the frequency band of 57 GHz to 71 GHz by a suitable replacement of the millimeter-wave transceiver. This expansion, coupled with the inclusion of additional channel metrics into our characterization efforts which will necessitate only modifications to our software, demonstrate the adaptability and potential of our testbed for addressing evolving research needs. Through this approach, we aspire to deepen our understanding of millimeter wave propagation characteristics, further informing the design and implementation of next-generation wireless networks in Colombia.

ACKNOWLEDGEMENT

This work was funded by Universidad Nacional de Colombia, sede Bogotá, in the framework of the HERMES-50848 project. Authors express their gratitude to David Mancipe from the Technological and Pedagogical University of Colombia (UPTC) for his contributions to the experimental testbed employed in this work.

REFERENCES

[1] Lee, W., *Wireless and Cellular Telecommunications*, McGraw-Hill, 2010.

[2] Rappaport, T. S., R. W. Heath Jr., R. C. Daniels, and J. N. Murdock, *Millimeter Wave Wireless Communications*, Pearson Education, 2015.

[3] Wen, Z. and H. Kong, "MmWave MIMO channel sounding for 5G," in *1st International Conference on 5G for Ubiquitous Connectivity*, 192–197, Akaslompolo, Finland, Nov. 2014.

[4] Rappaport, T. S., S. Sun, R. Mayzus, H. Zhao, Y. Azar, K. Wang, G. N. Wong, J. K. Schulz, M. Samimi, and F. Gutierrez, "Millimeter wave mobile communications for 5G cellular: It will work!" *IEEE Access*, Vol. 1, 335–349, 2013.

[5] Rappaport, T. S., G. R. MacCartney, M. K. Samimi, and S. Sun, "Wideband millimeter-wave propagation measurements and channel models for future wireless communication system design," *IEEE Transactions on Communications*, Vol. 63, No. 9, 3029–3056, 2015.

[6] Hindia, M. N., A. M. Al-Samman, T. A. Rahman, and T. M. Yazdani, "Outdoor large-scale path loss characterization in an urban environment at 26, 28, 36, and 38 GHz," *Physical Communication*, Vol. 27, 150–160, 2018.

[7] Ai, B., K. Guan, R. He, J. Li, G. Li, D. He, Z. Zhong, and K. M. S. Huq, "On indoor millimeter wave massive MIMO channels: Measurement and simulation," *IEEE Journal on Selected Areas in Communications*, Vol. 35, No. 7, 1678–1690, 2017.

[8] Papazian, P. B., C. Gentile, K. A. Remley, J. Senic, and N. Golmie, "A radio channel sounder for mobile millimeter-wave communications: System implementation and measurement assessment," *IEEE Transactions on Microwave Theory and Techniques*, Vol. 64, No. 9, 2924–2932, 2016.

[9] Chizhik, D., J. Du, R. Feick, M. Rodriguez, G. Castro, and R. A. Valenzuela, "Path loss and directional gain measurements at 28 GHz for non-line-of-sight coverage of indoors with corridors," *IEEE Transactions on Antennas and Propagation*, Vol. 68, No. 6, 4820–4830, 2020.

[10] Du, J., D. Chizhik, R. A. Valenzuela, R. Feick, G. Castro, M. Rodriguez, T. Chen, M. Kohli, and G. Zussman, "Directional measurements in urban street canyons from macro rooftop sites at 28 GHz for 90% outdoor coverage," *IEEE Transactions on Antennas and Propagation*, Vol. 69, No. 6, 3459–3469, 2021.

[11] Chizhik, D., J. Du, R. A. Valenzuela, D. Samardzija, S. Kucera, D. Kozlov, R. Fuchs, J. Otterbach, J. Koppenborg, P. Baracca, *et al.*, "Directional measurements and propagation models at 28 GHz for reliable factory coverage," *IEEE Transactions on Antennas and Propagation*, Vol. 70, No. 10, 9596–9606, 2022.

[12] Rubio, L., R. P. Torres, V. M. R. Peñarrocha, J. R. Pérez, H. Fernández, J.-M. Molina-Garcia-Pardo, and J. Reig, "Contribution to the channel path loss and time-dispersion characterization in an office environment at 26 GHz," *Electronics*, Vol. 8, No. 11, 1261, 2019.

[13] Rubio, L., V. M. R. Peñarrocha, M. Cabedo-Fabres, B. Bernardo-Clemente, J. Reig, H. Fernández, J. R. Pérez, R. P. Torres,

L. Valle, and O. Fernández, "Millimeter-wave channel measurements and path loss characterization in a typical indoor office environment," *Electronics*, Vol. 12, No. 4, 844, 2023.

[14] Arévalo, J. E., A. E. Núñez, C. A. Azurdia, J. L. Araque, and J. I. Sandoval, "Experimental indoor coverage of a commercial mm-Wave 5G network," in *2023 IEEE USNC-URSI Radio Science Meeting (Joint with AP-S Symposium)*, 13–14, Portland, OR, USA, Jul. 2023.

[15] Arévalo, J. E., A. E. Núñez, C. A. Azurdia, J. L. Araque, and J. I. Sandoval, "Experimental coverage measurements on a commercial 5G network in the 28 GHz mm-Wave band," in *2023 IEEE MTT-S Latin America Microwave Conference (LAMC)*, 65–67, San José, Costa Rica, Dec. 2023.

[16] Huang, J., Y. Liu, C.-X. Wang, J. Sun, and H. Xiao, "5G millimeter wave channel sounders, measurements, and models: Recent developments and future challenges," *IEEE Communications Magazine*, Vol. 57, No. 1, 138–145, 2019.

[17] Lin, Z., X. Du, H.-H. Chen, B. Ai, Z. Chen, and D. Wu, "Millimeter-wave propagation modeling and measurements for 5G mobile networks," *IEEE Wireless Communications*, Vol. 26, No. 1, 72–77, 2019.

[18] Järveläinen, J., K. Haneda, and A. Karttunen, "Indoor propagation channel simulations at 60 GHz using point cloud data," *IEEE Transactions on Antennas and Propagation*, Vol. 64, No. 10, 4457–4467, 2016.

[19] Wu, X., C.-X. Wang, J. Sun, J. Huang, R. Feng, Y. Yang, and X. Ge, "60-GHz millimeter-wave channel measurements and modeling for indoor office environments," *IEEE Transactions on Antennas and Propagation*, Vol. 65, No. 4, 1912–1924, 2017.

[20] Huang, J., C.-X. Wang, R. Feng, J. Sun, W. Zhang, and Y. Yang, "Multi-frequency mmWave massive MIMO channel measurements and characterization for 5G wireless communication systems," *IEEE Journal on Selected Areas in Communications*, Vol. 35, No. 7, 1591–1605, 2017.

[21] Rappaport, T. S., Y. Xing, G. R. MacCartney, A. F. Molisch, E. Mellios, and J. Zhang, "Overview of millimeter wave communications for fifth-generation (5G) wireless networks — With a focus on propagation models," *IEEE Transactions on Antennas and Propagation*, Vol. 65, No. 12, 6213–6230, 2017.

[22] METIS, "METIS channel models," May 2015.

[23] mmMAGIC, "6–100 GHz channel modelling for 5G: Measurement and modelling plans in mmMAGIC," May 2016.

[24] NYU Wireless, "Nyusim: The open source 5G channel model," May 2018.

[25] Fraunhofer Heinrich Hertz Institute, "Quasu deterministic radio channel generator," May 2017.

[26] MiWEBA, "Wp5: Propagation, antennas and multiantenna technique d5.1: Channel modeling and characterization," May 2014.

[27] 3rd Generation Partnership Project — 3GPP, "Study on channel model for frequencies from 0.5 to 100 GHz," May 2017.

[28] 3rd Generation Partnership Project — 3GPP, "Study on channel model for frequency spectrum above 6 GHz," Jun. 2017.

[29] Sivers Semicoductors, "Evaluation kits (EVK) and evaluation boards (EVB)," Dec. 2020.

[30] U-Blox, C94-M8P U-blox RTK Application Board Package. User Guide, 2017.

[31] Research, E., "Power level controls: Overview," https://files.ettus.com/manual/pagepower.html.